

Ectopic fat deposition contributes to age-associated pathology in *Caenorhabditis elegans*^S

Konstantinos Palikaras,^{1,*} Meropi Mari,^{1,*} Barbara Petanidou,^{†,§} Angela Pasparaki,^{*} George Filippidis,^{2,†} and Nektarios Tavernarakis^{2,***}

Institute of Molecular Biology and Biotechnology* and Institute of Electronic Structure and Laser,[†] Foundation for Research and Technology, Heraklion 71110, Crete, Greece; and Physics Department[§] and Medical School,** University of Crete, Heraklion 71003, Crete, Greece

ORCID IDs: 0000-0003-4748-5968 (G.F.); 0000-0002-5253-1466 (N.T.)

Abstract Age-dependent collapse of lipid homeostasis results in spillover of lipids and excessive fat deposition in nonadipose tissues. Ectopic fat contributes to lipotoxicity and has been implicated in the development of a metabolic syndrome that increases risk of age-associated diseases. However, the molecular mechanisms coupling ectopic fat accumulation with aging remain obscure. Here, we use nonlinear imaging modalities to visualize and quantify age-dependent ectopic lipid accumulation in *Caenorhabditis elegans*. We find that aging is accompanied by pronounced deposition of lipids in nonadipose tissues, including the nervous system. Importantly, interventions that promote longevity such as low insulin signaling, germ-line loss, and dietary restriction, which effectively delay aging in evolutionary divergent organisms, diminish the rate of ectopic fat accumulation and the size of lipid droplets. Suppression of lipotoxic accumulation of fat in heterologous tissues is dependent on helix-loop-helix (HLH)-30/transcription factor EB (TFEB) and autophagy. Our findings in their totality highlight the pivotal role of HLH-30/TFEB and autophagic processes in the maintenance of lipid homeostasis during aging, in addition to establishing nonlinear imaging as a powerful tool for monitoring ectopic lipid droplet deposition *in vivo*.—Palikaras, K., M. Mari, B. Petanidou, A. Pasparaki, G. Filippidis, and N. Tavernarakis. Ectopic fat deposition contributes to age-associated pathology in *Caenorhabditis elegans*. *J. Lipid Res.* 2017. 58: 72–80.

Supplementary key words aging • imaging • lipotoxicity • nonlinear phenomena • third harmonic generation • second harmonic generation

Some nematode strains used in this work were provided by the *Caenorhabditis Genetics Center*, which is funded by the National Center for Research Resources of the National Institutes of Health, and S. Mitani (National Bioresource Project) in Japan. This work was funded by grants from the European Research Council, the European Commission through the projects “LASERLAB-EUROPE IV - BIO-APP” (GA 654148) and REGPOT-2012-2013-1 and the Greek General Secretariat for Research and Technology. Dr. Konstantinos Palikaras is supported by a postdoctoral fellowship from the Bodossaki Foundation. The authors declare no competing financial interests.

Manuscript received 14 May 2016 and in revised form 6 November 2016.

Published, JLR Papers in Press, November 24, 2016
DOI 10.1194/jlr.M069385

Aging is accompanied by impairment of tissue-regenerative capacity and increased accumulation of lipids in nonadipose tissues and organs. Fat is stored in adipose tissue within specific cellular organelles, defined as lipid droplets. Lipid droplets are universal intracellular structures, evolutionary conserved from yeast to mammals (1, 2). They are composed of a phospholipid monolayer surface and a neutral lipid hydrophobic core. Several functional roles have been ascribed to lipid droplets, including most prominently energy storage, protection against excess lipid toxicity, and protein sequestration and degradation (1, 3). The enzymatic activity of several lipases located in the surface of lipid droplets, such as adipose triglyceride lipase and hormone sensitive lipase (4, 5), results in the production of FFAs. Those are substrates for β -oxidation enzymes residing in mitochondria and peroxisomes. However, overburdened adipose tissue causes a spillover of lipids and fat accumulation in nonadipose tissues, such as brain, liver, and cardiac and skeletal muscles. This is known as ectopic fat, and it is involved in the pathogenesis of metabolic syndrome (6, 7), a clustering of pathological conditions including type 2 diabetes, hypertension, and increased risk of cardiovascular diseases among others. Furthermore, obesity, hyperglycemia, elevated triglycerides, cholesterol and glucose blood levels, and high blood pressure are complex characteristics of metabolic syndrome. Ectopic fat is interspersed among normal cells of senescent tissues, and it can be found in multiple locations including skeletal and cardiac muscles, brown adipose tissue, bone marrow, and thymus (8–11). Ectopic fat accumulation contributes to organ dysfunction,

Abbreviations: CEPsh, cephalic sheath glial cells; GFP, green fluorescent protein; HLH, helix-loop-helix; HSD, honest significant difference; PMT, photomultiplier tube; SHG, second harmonic generation; TFEB, transcription factor EB; THG, third harmonic generation; TPEF, two-photon excited fluorescence.

¹K. Palikaras and M. Mari contributed equally to this article.

²To whom correspondence should be addressed.

e-mail: filip@iesl.forth.gr (G.F.); tavernarakis@imbb.forth.gr (N.T.)
^S The online version of this article (available at <http://www.jlr.org>) contains a supplement.

Copyright © 2017 by the American Society for Biochemistry and Molecular Biology, Inc.

This article is available online at <http://www.jlr.org>

specifically leading to impaired muscle strength and insulin resistance in skeletal muscles, reduced energy expenditure in brown adipose tissue, and impaired function of bone marrow stem cells (8, 12–15). Moreover, ectopic fat accrual is associated with systemic inflammation due to increased cytokine secretion from senescent ectopic adipocytes (16). The elucidation of the regulatory mechanisms orchestrating the interplay between aging and ectopic fat deposition has been an important focus of biomedical research during the last decades.

Most lipid research approaches rely on biochemical assays, such as gas chromatography or TLC (17–20). However, biochemical techniques pose several limitations and do not provide spatial information about the fat storage sites on whole animals. To alleviate these drawbacks, a plethora of fluorescent-based methods to investigate fat metabolism have been developed (21). Fluorescence imaging of live organisms by using dyes including Nile Red (22), Oil Red O (23, 24), BODIPY (18), and Sudan black (25), among others, are the most common, efficient, and widely used. The need for fast, noninvasive, label-free microscopy methods led to the development of coherent anti-Stokes Raman scattering (CARS) and stimulated Raman scattering (SRS) (26, 27). These methods allow lipid visualization without staining and provide valuable information about lipids chemical specificity and identity. However, CARS and SRS are laborious and costly microscopy methods as they require two tightly synchronized and perfectly aligned laser beams.

Second harmonic generation (SHG) and third harmonic generation (THG) are coherent nonlinear scattering phenomena. The SHG signal is produced from noncentrosymmetric molecules, and its signal arises from structures with a high degree of orientation and organization but without inversion symmetry, for instance myosin thick filaments, collagen, microtubules, or lipid membranes (28–31). On the other hand, THG is sensitive to local differences in third-order nonlinear susceptibility $\chi^{(3)}$, refractive index, and dispersion. Under tight focusing conditions, the extent of THG signal increases dramatically when beam focus spans an interface between two optically different materials. In THG microscopy, the contrast arises from interfaces and optical heterogeneities of size comparable to beam focus. No THG signal is collected when the laser beam is focused into a homogeneous, normally dispersive medium (32).

Higher harmonic generation imaging techniques (SHG, THG) constitute powerful tools for elucidating subcellular structures and anatomical changes of various biological samples and monitoring complicated developmental processes in vivo at microscopic level (33–35). Furthermore, THG is a reliable, nondestructive, label-free method for imaging lipid deposition in tissues and cells of various biological samples (36). This modality is used for precise identification of lipid deposition in the nematode *Caenorhabditis elegans* (37, 38). By using this diagnostic technique, it is feasible to visualize and monitor the concentration of lipids in adipose and muscular tissues of wild-type animals. Adipose fat content markedly increases during development, followed by subsequent gradual reduction during adulthood (38), while ectopic fat deposition increases with age (37).

However, the regulatory mechanisms dictating lipid homeostasis collapse and ectopic fat deposition during aging still remain elusive.

Here we report the use of SHG and THG noninvasive and label-free imaging techniques to monitor and quantify ectopic lipid deposition and delineate the precise connection between ectopic fat accumulation and aging. Our studies suggest that fat content is gradually accrued with age in nonadipose tissues, such as body wall muscles, pharyngeal muscles, and neurons of *C. elegans*, independently of growing temperature. Importantly, several genetic interventions known to delay aging across species such as low insulin signaling, germ-line loss, and caloric restriction alleviate ectopic fat levels and reduce lipid droplet size. Interestingly, autophagy and helix-loop-helix (HLH)-30, the mammalian homolog of transcription factor EB (TFEB) in nematodes, are required to prevent ectopic fat accumulation. Our findings highlight the pivotal role of HLH-30/TFEB in metabolism and prevention of ectopic fat expansion, thereby preserving organismal homeostasis during aging.

MATERIALS AND METHODS

Nonlinear microscopy setup

The experimental setup was similar to the one described in our previous studies (37, 38). A Yb-based solid-state femtosecond laser oscillator, emitting near infrared pulsed light at a central wavelength of 1,028 nm (t-pulse, Amplitude systems, 200 fs, 50 MHz 1 W) is used as excitation source. The laser beam is guided to a modified upright microscope (Nikon Eclipse ME600D). Adjustable neutral density filters (New Focus) are utilized to control the power at the sample plane. A telescope system is used to control the beam radius. A set of galvanometric mirrors (Cambridge Technology) is used to perform the fast raster scanning in the selected xy plane of the *C. elegans* sample. The focal plane is adjusted by using a motorized translation stage (Standa Ltd., 1 μ m minimum step). Diffraction limited focusing is achieved by using a high numerical aperture objective lens (Carl Zeiss, C-Achroplan 32 \times , NA 0.85, water immersion). Specimens are placed between two thin (\sim 70 μ m) glass coverslips (Marienfeld). The glass slides are separated by a 100 μ m spacer in order to protect the samples. Our experimental apparatus allows the collection of two different nonlinear optical signals simultaneously (one in the reflection and the other in the transmission mode). For our experiments, THG is detected in the forward path, while SHG and two-photon excited fluorescence (TPEF) signals are detected in the backscattered direction in distinct set of measurements. This quality of our system makes it capable of performing colocalization measurements. Sample scanning and data acquisition are controlled through a LabVIEW interface adapted to the experiment requirements. The bright field observation of the worm is performed via a CCD camera (PxeLINK). The signals in the reflection mode (SHG or TPEF) are recorded by a photomultiplier tube (PMT; Hamamatsu) that is attached on the microscope eyepiece site and wired to the computer. An appropriate narrow bandpass interference filter (CVI F03, 514.5 nm) is used in the case of SHG measurements. For the TPEF measurements, a short pass filter (SPF 700 nm, CVI) and a bandpass filter (640 nm/40 nm, Chroma), are used for the Nile Red staining of the samples while for the green fluorescent protein (GFP) staining a long pass filter (FGL530 Thorlabs) is used. On the other hand, for the forward detected

THG signals a condenser lens (Carl Zeiss, PlanNeofluar, 40 \times , 0.75 NA, air immersion), a colored glass filter (U 340-Hoya), and a second PMT (Hamamatsu) are used. The laser power on the sample plane was 48 mW for all measurements (\sim 1 nJ per pulse). Our setup scans 500 \times 500 pixels THG, SHG, or TPEF image in 1 s. To improve the signal to noise ratio (SNR), 30 scans are averaged for each final image. To further improve image quality, a series of 2D optical sections was acquired at 2 μ m intervals (z stack) and projected (maximum intensity projection) onto a single plane. Image J is used for viewing and processing the obtained data (National Institutes of Health; <http://imagej.nih.gov/ij/>).

Imaging and statistical analysis

All the samples have been imaged under constant irradiation conditions. THG intensity values were collected from the PMTs and were stored in 2D 500 by 500 matrices, representing each slice image of the animal. THG signal quantification was performed by setting a threshold in the obtained normalized slice images, so that regions generating high levels of nonlinear signal (mainly corresponding to lipid particles) are solely detected and isolated. Processing of images and thresholding was performed using Image J. Normalized 8 bit slice images of the sample are initially inserted in Image J and consequently thresholded using a constant threshold value so that only the highest 23.5% of the THG signals is recorded and quantified. In this manner, the generated stack of binary images following the thresholding procedure represents exclusively the lipid droplets in the pharyngeal area of the animal, while the lower THG signals arising from other inhomogeneous structures are effectively eliminated. Lipid content was measured by calculating the total area of detected regions for all sequential optical planes covering the sample depth. In addition, the average lipid droplet size for each animal can be estimated through the same process and compared among the different strains. At least 12 animals were imaged for each genetic background or time point examined. Mean pixel intensities were calculated by averaging values obtained for each image, after thresholding, in Image J. Detection and area measurement of lipid droplet regions in the resulting binary images stack were performed through the Analyze Particles function of Image J. The total sum of the detected areas (in pixels) was calculated as a representative index of the total lipid content within the examined part of the pharynx. Furthermore, the average lipid droplet size for each animal was also calculated using the same data. Total lipid particle area and average lipid droplet size (μ m²) measurements of different samples were compared by one-way ANOVA, followed by Tukey honest significant difference (HSD) post hoc tests (SPSS, IBM Corp.).

C. elegans strains and culture methods

We followed standard procedures for *C. elegans* strain maintenance (39). Nematode rearing temperature was kept at 20°C, unless noted otherwise. The following strains were used in this study: N2: wild-type Bristol isolate, CB1189: *unc-51(e1189)V*, CB1370: *daf-2(e1370)III*, CB4037: *glp-1(e2141)III*, DA465: *eat-2(ad465)II*, *lgg-2(tm5755)IV*, *lipl-4(tm4417)V*, *lipl-1(tm1954)* *lipl-3(tm4498)V*. To investigate whether THG signal arises from lysosomes, we used the following transgenic animal: RT258: *unc-119(ed3)III*; *pw1s50*[*p_{lmp-1}*:LMP-1::GFP + *Cbr-unc-119(+)*]. We used IR28: N2;*Is001*[*p_{myo-3}*:MYO-3::GFP] to monitor body wall muscle cells. The following strains were used for monitoring ectopic fat depositions in nervous system: BZ555: N2;*egIs1*[*p_{dat-1}*:GFP], IR824: N2;*Ex001*[*p_{hth-17}*:GFP], and IR1886: *hth-30(tm1978)*;*Ex001*[*p_{hth-17}*:GFP].

Molecular cloning

To generate the *p_{hth-17}*-GFP reporter construct, we fused a *SalI*/*KpnI* fragment, containing the sequence of *hth-17* promoter,

amplified from *C. elegans* genomic DNA using the primers 5'ACGCGTCCGACATGACGGAGTTGAGGCCAAAATCC3' and 5'CGGGGTACCGACTGGGGTGTAAAGTGAATGAGAGAGGA3', at the amino (N) terminus of GFP, in the pPD95.77 plasmid vector. The *p_{hth-17}*-GFP reporter construct was coinjected with pRF4 (contains the *rol-6(su1006)* dominant transformation marker) into the gonads of wild-type animals. For engineering the *lipl-4* and *hth-30* RNAi construct, gene-specific fragments of interest were obtained by PCR amplification directly from *C. elegans* genomic DNA using the following sets of primers 5'CTACAACACAACAACAAAAGAT3' and 5'ATGAGAAAGAAATTACCTGAAC3' and 5'TTGACATTCCAAACGAGACGC3' and 5'TGCTCGTCCCTAGAATTCAACA3', respectively. The *lgg-1* and *bec-1* RNAi constructs have been described previously (40).

Fat staining

For Nile Red staining, L4-stage worms were incubated on plates seeded with OP50 bacteria and transferred to fresh plates every other day until they reached day 1 or day 12 of adulthood. Then, worms were fixed for 5 min in 3 ml cold (-20° C) methanol. Subsequently, 2 ml of PBS-T (PBS with 0.1% Tween-20) were added and tubes were centrifuged for 2 min at 3,000 rpm to remove the supernatant. Finally, worms were washed twice in PBS-T. Following fixation, worms were stained for 20 min in 10 mM Nile Red (Sigma-Aldrich Corp.), added from a stock solution of 50 mM Nile Red diluted in 100% DMSO. For SHG and THG imaging microscopy, nematodes were collected and washed with M9 buffer several times to remove bacteria. Prior to imaging, worms were immobilized with sodium azide buffer at a final concentration of 10 mM. Finally, immobilized animals were examined microscopically.

BODIPY uptake assay

One-day-old and 5-day-old adults were placed on nematode growth media *Escherichia coli* (OP50) plates seeded with 100 μ l of 5 μ M C1BODIPY-C12 (Invitrogen, D3823) diluted in M9 buffer. Animals were incubated for 1 h with the compound at room temperature. Stained and washed worms were immobilized with levanisole before mounting on 2% agarose pads for microscopic examination with a Zeiss AxioImager Z2 epifluorescence microscope. We calculated the mean and maximum pixel intensity for each animal in these images using the ImageJ software (<http://rsb.info.nih.gov/ij/>). In each experiment, at least 90 animals were examined for each strain/condition. Each assay was repeated at least three times. We used the Prism software package (GraphPad Software) for statistical analyses.

RESULTS

Nonlinear modalities as diagnostic tools for visualization and quantification of ectopic fat in *C. elegans*

We utilized nonlinear imaging methods to visualize and quantify ectopic fat deposition in *C. elegans*. The nematode has been established as a model organism for dissection of molecular mechanisms regulating lipid metabolism due to its genetic tractability and transparency throughout its life cycle (41, 42). A combination of THG and TPEF modalities allowed the detection of THG signals from lipid droplets stored in nonadipose tissues. We imaged worms fixed and stained with Nile Red, a fluorescent dye routinely used for fat content visualization (21, 23). In Fig. 1, the contour, the shape, the linings of the animal pseudocoelomic cavity,

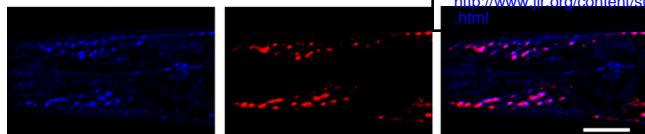


Fig. 1. THG specifically visualizes ectopic fat deposition in *C. elegans*. THG signals (blue) colocalize with Nile Red (red) labeled lipids in *C. elegans*, visualized by TPEF. Images of pharyngeal area of 1-day-old wild-type animals are shown. Scale bar denotes 30 μm .

and other discontinuities in the anterior body segment are detected through THG measurements (blue). The highest THG signals arise from internal structures of the head region. We found that these high-intensity THG (blue) structures and TPEF (Nile Red, red) signals colocalized (purple) in the pharyngeal region of fixed animals, indicating unambiguously that strong THG signal emanates from ectopically distributed lipid droplets (Fig. 1; supplemental Fig. S1A–D). For the colocalization measurements, central slices of the worm were used to avoid the contribution of the lipids from the hypodermis. The fluorescence might be more intense compared with the THG on some structures resulting in the red overwhelming TPEF. Subtle or no changes in the intensity or localization of THG signals collected from muscular areas were monitored in animals stained with Nile Red (Fig. 1; supplemental Fig. S1A–D). Additionally, we used transgenic animals expressing the myosin heavy chain, MYO-3, tagged with GFP in body wall muscle cells and THG imaging to monitor lipid droplets distribution in muscular area. Lipid droplets (internal circular structures in blue) were detected in striated body wall muscle cells, verifying the existence of ectopic fat deposition in *C. elegans* (supplemental Fig. S2). To validate the specificity of THG signal and investigate whether it derives from lysosome-related structures, we imaged transgenic animals expressing the lysosomal protein LMP-1 fused with GFP. We found that THG signal is clearly distinct from lysosomes (supplemental Fig. S3). Moreover, lipofuscin autofluorescence does not overlap with THG signals (38).

Previous studies have shown enhanced ectopic lipid deposition during aging in nematodes (37, 43). Simultaneous measurements of SHG and THG were performed on the whole body of wild-type *C. elegans* to monitor and compare ectopic fat storage in young and old animals. We found that fat deposition increases in body wall muscle cells with age (Fig. 2A). The intestine and hypodermis are the main lipid storage tissues of nematodes; hence, imaging of lipid droplets in intestinal cells has been used for the identification of genes regulating lipid metabolism (25). Subsequently, we focused on the pharynx, an organ composed of eight layers of muscles, to quantify ectopic fat levels and avoid THG signal arising from intestinal area. We observed that ectopic lipids gradually increase in pharyngeal muscles of wild-type nematodes during aging (Fig. 2B, C; supplemental Fig. S4). Although temperature influences *C. elegans* physiology and metabolic rate, lipids expand ectopically in a temperature-independent manner. Age-matched animals raised at different growing temperatures (15°C, 20°C, and 25°C) display similar ectopic fat levels throughout life (supplemental Fig. S5).

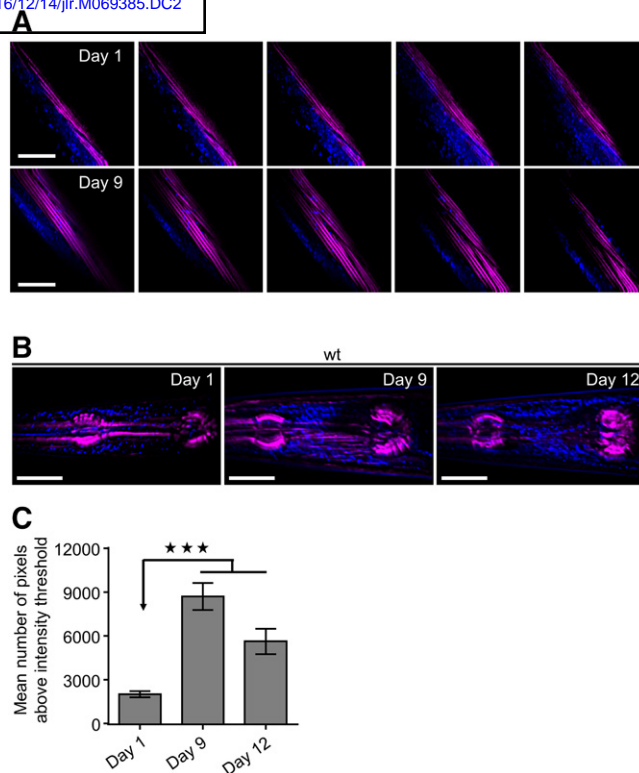


Fig. 2. SHG and THG imaging reveal ectopic lipid droplet accumulation during aging. Simultaneous SHG (magenta) and THG (blue) signals visualize fat storage in body wall muscles (z-sequence of 2D slices divided by 2 μm) (A) and z-projections to maximum intensity of 15 slices divided by 2 μm of pharyngeal muscles (B) of wild-type nematodes during aging. C: Quantification of THG signals. $n = 12$ for each time point. *** $P < 0.001$, one-way ANOVA followed by Tukey HSD post hoc test; error bars denote standard error of the mean. Scale bars denote 30 μm .

Recently, it was documented that mice fed with a high-fat diet display excessive lipid content in hypothalamic brain region (44). Ectopic fat in the brain could impair neuronal function and contribute to manifestation of neurological disorders. We used nonlinear modalities to investigate whether fat accumulates in *C. elegans* nervous system. Nonneuronal glial cells play a pivotal role in nervous system, supporting neuronal activity through their metabolic and structural function and influencing animal behavior. Recently, it was reported that neuronal dysfunction leads to lipid droplet accrual in neighboring glial cells altering, in turn, their lipid metabolism and causing neurodegeneration (45). Cephalic sheath glial cells (CEPsh) are located in the anterior part of the pharynx forming a tubular structure, which regulates neuronal organization, axon guidance, and dendrite and axon extension. Ablation of CEPsh during embryonic development results in impaired nerve ring structure and axon guidance defects (46, 47). Coupling of both THG and TPEF methods revealed lipid droplet accumulation in CEPsh during aging (Fig. 3A, B). CEPsh surround the sensory ending of CEP (neurons associated with cephalic sensilla) dopaminergic neurons. By using transgenic animals expressing GFP fluorescent protein in CEPs, ADEs (sensory neurons of anterior deirids),

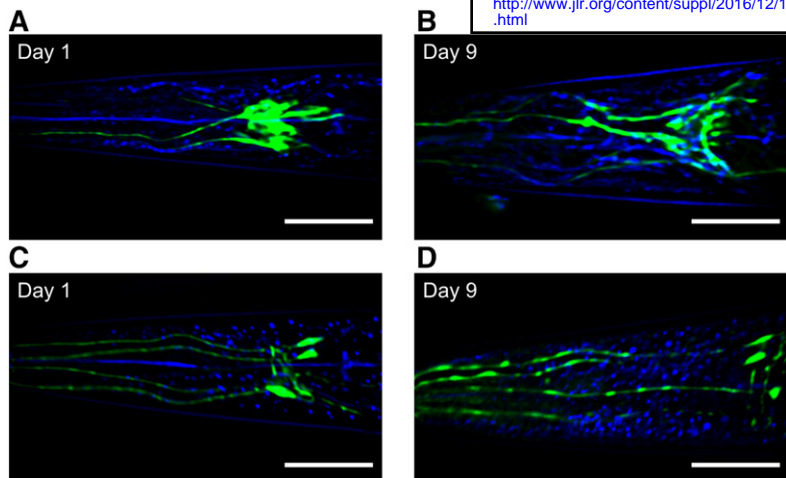


Fig. 3. Gradual lipid droplet accumulation in *C. elegans* nervous system with age. Coupling of TPEF (green) and THG (blue) imaging reveals lipid droplet accumulation in CEPsh (A, B) and around neuronal cell bodies and along neuronal processes of CEP dopaminergic neurons (C, D) during aging. The images are z-projections of 18 slices to maximum intensity divided by 2 μm . Scale bars denote 30 μm .

PDEs (neurons with ciliated endings in the posterior deirid sensilla) dopaminergic neurons, we monitored age-dependent accrual of lipid droplets around neuronal cell bodies and along neuronal processes (Fig. 3C, D).

Taken together, our results suggest that fat content gradually increases in several nonadipose tissues, such as body wall muscles, pharyngeal muscles, and neuronal and glial cells during aging in *C. elegans*. Moreover, our study establishes nonlinear phenomena as a novel, noninvasive, and label-free microscopy method to visualize ectopic lipid deposition in vivo.

Longevity-promoting interventions alleviate the rate of age-dependent ectopic fat accumulation and reduce lipid droplet size in *C. elegans*

Restriction of calorie intake prolongs life span in many species including rats, mice, fish, worms, flies, and yeast (48). This dietary manipulation is referred as caloric restriction. In mammals, nutrient deprivation results in the delay of numerous detrimental age-associated hallmarks, such as increased adiposity, abdominal fat, and impaired hepatic and peripheral insulin action (49, 50). Although caloric restriction effect on primate life span remains ambiguous, its beneficial impact on preventing a variety of age-related pathologies is generally accepted (51–53).

In *C. elegans*, caloric restriction can be genetically mimicked with *eat-2(ad465)* mutants, which display defective food intake due to reduced pumping rate (54). Consistent with the previous reported effects of caloric restriction on ectopic fat deposition (49, 50), *eat-2(ad465)* animals display decreased rate of ectopic lipid storage in pharyngeal muscles compared with their wild-type counterparts during aging (Fig. 4A, B). Interestingly, EAT-2-depleted animals display steady levels of ectopic lipids throughout life (supplemental Fig. S6A, B). In addition to caloric restriction, we found that low insulin signaling and germ-line loss diminish the rate of ectopic fat accumulation during aging (Fig. 4A; supplemental Fig. S6C). Furthermore, the size of lipid droplets is significantly reduced in long-lived mutants compared with wild-type animals (Fig. 4B). Increased longevity of *eat-2(ad465)* mutants is mediated by HLH-30 transcriptional activity (23, 55). HLH-30 is the mammalian

homolog of the basic HLH/TFEB, which coordinates the expression of several lysosomal and autophagy genes (56). To investigate the contribution of HLH-30 activity in regulation of age-dependent ectopic fat deposition, we knocked down HLH-30 in wild-type and *eat-2(ad465)* mutants. Notably,

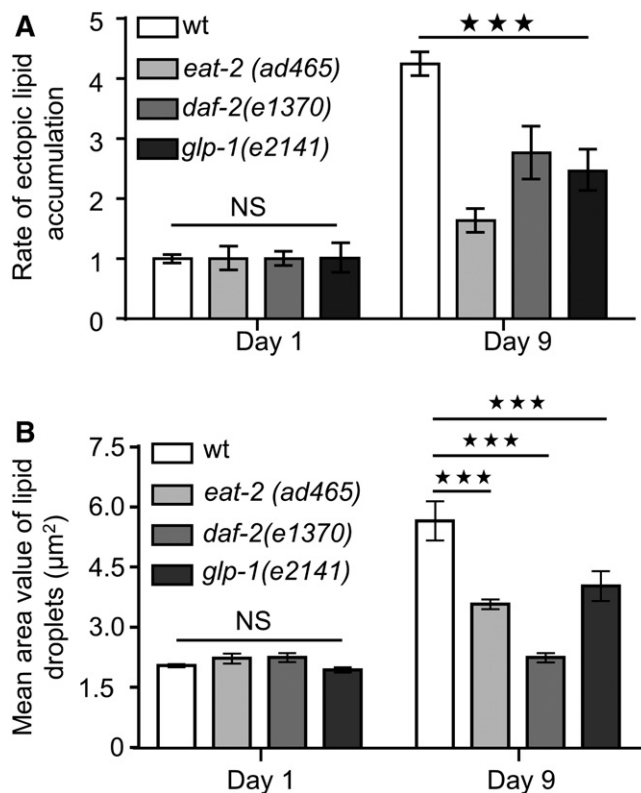


Fig. 4. Longevity-promoting interventions prevent age-dependent ectopic fat deposition. A: The rate of ectopic lipid content in the pharynx of wild-type animals is significantly increased compared with *eat-2(ad465)*, *daf-2(e1370)*, and *glp-1(e2141)* mutants during aging. The division of THG signal values, at day 1 and day 9, by the day 1 THG signal values of each strain, respectively, depicts the rate of ectopic lipid content. B: Quantification of lipid droplet sizes in long-lived animals during aging. $n = 12$ for each genetic background and time point. NS, $P > 0.05$, *** $P < 0.001$, one-way ANOVA followed by Tukey HSD post hoc test; error bars denote standard error of the mean.

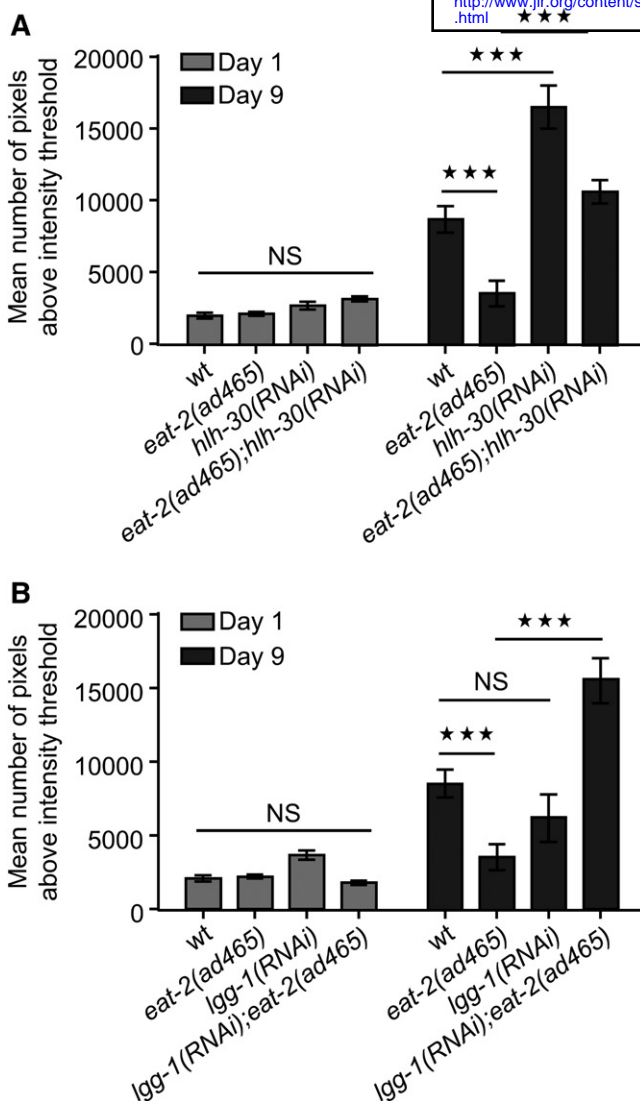


Fig. 5. HLH-30 and autophagy preserve lipid homeostasis in *eat-2(ad465)* mutants. A, B: Quantification of THG signals in the pharyngeal muscle cells of wild-type and *eat-2(ad465)* animals upon knockdown of (A) *hlh-30* or (B) *lgg-1*. $n = 12$ for each genetic background and time point. NS, $P > 0.05$, *** $P < 0.001$, one-way ANOVA followed by Tukey HSD post hoc test; error bars denote standard error of the mean.

HLH-30 depletion leads to excessive ectopic lipid expansion both in wild-type and *eat-2(ad465)* animals (Fig. 5A; supplemental Fig. S7A) without influencing their feeding behavior (supplemental Fig. S7B). Additionally, lipid droplets are enlarged upon knocking down of HLH-30 in *eat-2(ad465)* animals (supplemental Fig. S8A), underlining the essential role of HLH-30 in the regulation of ectopic fat deposition.

HLH-30/TFEB is considered as the master regulator of autophagy (57). Autophagy is a core catabolic process, which removes toxic protein aggregates and/or damaged organelles, thus preserving cellular and organismal homeostasis and supplying cells with recycled amino acids for anabolism (58). A recent study demonstrated the vital role of autophagy in lipid homeostasis of nematodes highlighting its necessity in lipid storage and energy metabolism (59).

Autophagy is required for increased longevity of *eat-2(ad465)* mutants (60). Although autophagy inhibition does not alter ectopic fat accumulation in nonstress conditions during aging (supplemental Figs. S8B and S9A), knockdown of *lgg-1* encoding the *C. elegans* homolog of the mammalian LC3 results in enhanced lipid levels and increased lipid droplet size in pharyngeal muscles of *eat-2(ad465)* animals (Fig. 5B; supplemental Fig. S8B). These results suggest that HLH-30 regulates ectopic fat in an autophagy-independent manner in nonstressed wild-type nematodes because autophagy differentially affects lipid distribution under normal and dietary-restricted conditions. HLH-30 is known to govern lysosomal activity through the transcriptional regulation of several lysosomal genes (23, 55–57). Lysosomal acid lipases catabolize lipid droplets and modulate fat content. To investigate whether lysosomal acid lipases are involved in the regulation of ectopic fat, we monitored fat content in pharyngeal muscles of *lipl-4(tm4417)* and *lipl-1(tm1954) lipl-3(tm4498)* mutants. LIPL-4, a lysosomal triglyceride lipase, is associated with life span extension and modulation of lipid metabolism (61–63). However, neither LIPL-4 nor simultaneous LIPL-1 and LIPL-3 inhibition affects ectopic fat distribution in nonstressed wild-type animals during aging (supplemental Fig. S9B). Interestingly, LIPL-4 depletion results in excessive ectopic fat accumulation and enlargement of lipid droplets in *eat-2(ad465)* mutants (supplemental Fig. S10A, B). Considering the function of HLH-30/TFEB in multiple metabolic pathways mediating both breakdown and biosynthesis of lipids (64), our results suggest the existence of an alternative redundant mechanism involved in the maintenance of lipid homeostasis under nonstress conditions during aging. A very recent study uncovered the role of vitellogenins/lipoproteins in autophagy-mediated longevity (65). Age-dependent vitellogenin/lipoprotein accumulation could drive ectopic lipid deposition during aging. Several transcription factors known to promote longevity, including DAF-16/FOXO and SKN-1/Nrf, among others, regulate vitellogenins, thus maintaining lipid homeostasis (65, 66). In addition, HLH-30/TFEB could preserve lipid homeostasis through vitellogenins/lipoproteins regulation.

DISCUSSION

Nonlinear phenomena are established microscopy techniques for visualization of subcellular structures and biological processes in vivo. In this study, we show that *C. elegans* ectopic fat can be monitored and quantified accurately by combining noninvasive, label-free nonlinear imaging modalities. Lipid metabolism is altered during aging and is mainly characterized by elevated cholesterol levels, reduced fatty acid oxidation, increased lipogenesis and impaired lipolysis (65, 67, 68). Age-dependent alterations of fat storage can promote lipotoxic effects resulting in tissue homeostasis collapse and eventually death (43). FFAs per se or FFAs-derived metabolites stimulate cell death pathways or oxidative stress undermining cellular activity and

survival (69–72). In this study, we combined SHG with THG and showed that lipids expand ectopically in pharyngeal and body wall muscle cells during aging in *C. elegans* animals. Furthermore, our method provides novel insights into ectopic fat distribution in glial and neuronal cells. Although lipid storage and metabolism is essential for proper function of nervous system, our findings are consistent with several recent studies proposing that aberrant lipid droplet formation and expansion could contribute to neurodegeneration and development of neurological disorders (3, 73–76).

As life expectancy and standards of living are constantly improving in modern societies worldwide, the proportion of aged individuals will increase significantly over the next decades. In parallel, incidences of age-associated disorders, such as obesity, diabetes, cardiovascular pathologies, sarcopenia, osteoporosis, and cancer, which already raise health system costs worldwide, will increase. Calorie deprivation, either by decreasing food intake or by using caloric restriction mimetics, is the only nongenetic intervention promoting longevity and protecting against age-related pathologies, including metabolic syndrome among others (51, 77). Metabolic syndrome affects a significant percent of adult population in developed countries. Affected individuals display greater risk for developing type 2 diabetes, increased inflammation, cognitive impairment, and accelerated functional decline (78, 79). Caloric restriction delays or prevents several potentially harmful age-associated phenotypes, which are known to be involved in metabolic syndrome progression (49, 50). To this direction, we observed decreased levels of ectopic fat deposition in caloric-restricted *eat-2(ad465)* mutants compared with wild-type nematodes during aging. Notably, autophagy and HLH-30/TFEB are indispensable for reduced ectopic fat levels in caloric-restricted animals. This excessive ectopic lipid accumulation can be explained by either a cell autonomous inability to hydrolyze lipids via lysosomal lipases and lipophagy in peripheral tissues or a cell autonomous enhanced uptake of lipids by nonadipose tissues or a cell nonautonomous elevated lipid secretion toward peripheral tissues. Interestingly, autophagy depletion does not lead to excessive fat accumulation in nonadipose tissues of wild-type nematodes under normal conditions, similarly to HLH-30 deficiency. These results indicate that HLH-30 regulates lipid metabolism and prevents ectopic fat deposition in an autophagy-independent manner. HLH-30/TFEB is known to control autophagy through transcriptional regulation of several lysosomal and autophagy genes (23, 55–57). Because autophagy is not implicated in the regulation of ectopic lipid distribution in nonstress conditions, HLH-30 might coordinate lipid metabolism by modulating lysosomal function. Although lysosomal lipase inhibition results in elevated ectopic fat deposition in caloric-restricted *eat-2(ad465)* animals, deficiency of lysosomal lipases does not enhance ectopic lipid storage in wild-type nematodes during aging, underlining the existence of an alternative regulatory mechanism of ectopic fat distribution under nonstress conditions.

Recently, it was suggested that age-dependent increase of the vitellogenin/lipoprotein expression levels could

promote excessive lipid accrual in other tissues (65). Several transcription factors, which are known to induce longevity such as DAF-16, PHA-4, and SKN-1 among others, also regulate the expression levels of vitellogenins, thereby preserving lipid homeostasis (65, 66). HLH-30/TFEB could also be involved in the regulation of vitellogenins/lipoproteins modulating lipid homeostasis and ectopic lipid storage under normal and stress-induced conditions. Although HLH-30/TFEB is required under stress conditions to maintain organismal homeostasis and survival (55, 80), its function is not restricted to normal conditions. Wild-type nematodes subjected to RNAi against *hlh-30* display decreased expression of several autophagy and lysosomal genes. Additionally, HLH-30/TFEB is present in the nucleus even under normal conditions (55) indicating its role in basal autophagy in nonstressed animals. However, the impact of HLH-30/TFEB activity in the vitellogenin/lipoprotein regulation needs further to be examined.

Investigating the interplay between aging and ectopic lipid accumulation will enlighten new avenues for therapeutic interventions to cure metabolic syndrome-associated pathologies. Therefore, the development and establishment of novel, noninvasive, and label-free methods for visualizing fat deposition in vivo is a prerequisite to tackle the demand of fatty acids imaging distribution. Nonlinear imaging phenomena are successfully used for in vivo visualization of lipid storage and ectopic fat deposition. Nonlinear microscopes are readily used systems and require just a single pulsed femtosecond laser light source, in contrast to other more laborious label-free microscopy techniques. Furthermore, nonlinear modalities (SHG, THG) can be implemented by easily upgrading a common multiphoton microscope. These specific advantages render nonlinear imaging methods, and specifically THG modality, versatile, reliable, and easily accessible tools for the dissection of cellular and molecular mechanisms regulating lipid storage and metabolism.

The authors thank N. Kourtis for the *C. elegans* strain expressing GFP in CEPsh, E. J. O'Rourke for *lipl-1(tm1954) lipl-3(tm4498) C. elegans* strain, and A. Fire for plasmid vectors.

REFERENCES

1. Farese, R. V., Jr., and T. C. Walther. 2009. Lipid droplets finally get a little R-E-S-P-E-C-T. *Cell*. **139**: 855–860.
2. Kühnlein, R. P. 2012. Lipid droplet-based storage fat metabolism in *Drosophila*. Thematic review series: lipid droplet synthesis and metabolism: from yeast to man. *J. Lipid Res.* **53**: 1430–1436.
3. Welte, M. A. 2015. Expanding roles for lipid droplets. *Curr. Biol.* **25**: R470–R481.
4. Egan, J. J., A. S. Greenberg, M. K. Chang, S. A. Wek, M. C. Moos, Jr., and C. Londos. 1992. Mechanism of hormone-stimulated lipolysis in adipocytes: translocation of hormone-sensitive lipase to the lipid storage droplet. *Proc. Natl. Acad. Sci. USA.* **89**: 8537–8541.
5. Zimmermann, R., J. G. Strauss, G. Haemmerle, G. Schoiswohl, R. Birner-Gruenberger, M. Riederer, A. Lass, G. Neuberger, F. Eisenhaber, A. Hermetter, et al. 2004. Fat mobilization in adipose tissue is promoted by adipose triglyceride lipase. *Science*. **306**: 1383–1386.
6. Ackerman, D., and D. Gems. 2012. The mystery of *C. elegans* aging: an emerging role for fat. Distant parallels between *C. elegans* aging and metabolic syndrome? *BioEssays*. **34**: 466–471.

7. Le Lay, S., and I. Dugail. 2009. Connecting lipid droplet biology and the metabolic syndrome. *Prog. Lipid Res.* **48**: 191–195.
8. Kuk, J. L., T. J. Saunders, L. E. Davidson, and R. Ross. 2009. Age-related changes in total and regional fat distribution. *Ageing Res. Rev.* **8**: 339–348.
9. Saely, C. H., K. Geiger, and H. Drexel. 2012. Brown versus white adipose tissue: a mini-review. *Gerontology.* **58**: 15–23.
10. Sepe, A., T. Tchkonja, T. Thomou, M. Zamboni, and J. L. Kirkland. 2011. Aging and regional differences in fat cell progenitors – a mini-review. *Gerontology.* **57**: 66–75.
11. Youm, Y. H., H. Yang, R. Amin, S. R. Smith, T. Leff, and V. D. Dixit. 2010. Thiazolidinedione treatment and constitutive-PPARgamma activation induces ectopic adipogenesis and promotes age-related thymic involution. *Ageing Cell.* **9**: 478–489.
12. Mattson, M. P. 2010. Perspective: does brown fat protect against diseases of aging? *Ageing Res. Rev.* **9**: 69–76.
13. Rosen, C. J., C. Ackert-Bicknell, J. P. Rodriguez, and A. M. Pino. 2009. Marrow fat and the bone microenvironment: developmental, functional, and pathological implications. *Crit. Rev. Eukaryot. Gene Expr.* **19**: 109–124.
14. Rosen, C. J., and M. L. Boussein. 2006. Mechanisms of disease: is osteoporosis the obesity of bone? *Nat. Clin. Pract. Rheumatol.* **2**: 35–43.
15. Tchkonja, T., D. E. Morbeck, T. Von Zglinicki, J. Van Deursen, J. Lustgarten, H. Scoble, S. Khosla, M. D. Jensen, and J. L. Kirkland. 2010. Fat tissue, aging, and cellular senescence. *Ageing Cell.* **9**: 667–684.
16. Cartwright, M. J., T. Tchkonja, and J. L. Kirkland. 2007. Aging in adipocytes: potential impact of inherent, depot-specific mechanisms. *Exp. Gerontol.* **42**: 463–471.
17. Brooks, K. K., B. Liang, and J. L. Watts. 2009. The influence of bacterial diet on fat storage in *C. elegans*. *PLoS One.* **4**: e7545.
18. Mak, H. Y., L. S. Nelson, M. Basson, C. D. Johnson, and G. Ruvkun. 2006. Polygenic control of *Caenorhabditis elegans* fat storage. *Nat. Genet.* **38**: 363–368.
19. Watts, J. L., and J. Browse. 2002. Genetic dissection of polyunsaturated fatty acid synthesis in *Caenorhabditis elegans*. *Proc. Natl. Acad. Sci. USA.* **99**: 5854–5859.
20. Watts, J. L., and J. Browse. 2006. Dietary manipulation implicates lipid signaling in the regulation of germ cell maintenance in *C. elegans*. *Dev. Biol.* **292**: 381–392.
21. Elle, I. C., L. C. Olsen, D. Pultz, S. V. Rodkaer, and N. J. Faergeman. 2010. Something worth dying for: molecular tools for the dissection of lipid metabolism in *Caenorhabditis elegans*. *FEBS Lett.* **584**: 2183–2193.
22. Greenspan, P., E. P. Mayer, and S. D. Fowler. 1985. Nile red: a selective fluorescent stain for intracellular lipid droplets. *J. Cell Biol.* **100**: 965–973.
23. O'Rourke, E. J., and G. Ruvkun. 2013. MXL-3 and HLH-30 transcriptionally link lipolysis and autophagy to nutrient availability. *Nat. Cell Biol.* **15**: 668–676.
24. O'Rourke, E. J., A. A. Soukas, C. E. Carr, and G. Ruvkun. 2009. *C. elegans* major fats are stored in vesicles distinct from lysosome-related organelles. *Cell Metab.* **10**: 430–435.
25. Ashrafi, K., F. Y. Chang, J. L. Watts, A. G. Fraser, R. S. Kamath, J. Ahringer, and G. Ruvkun. 2003. Genome-wide RNAi analysis of *Caenorhabditis elegans* fat regulatory genes. *Nature.* **421**: 268–272.
26. Hellerer, T., C. Axang, C. Brackmann, P. Hillertz, M. Pilon, and A. Enejder. 2007. Monitoring of lipid storage in *Caenorhabditis elegans* using coherent anti-Stokes Raman scattering (CARS) microscopy. *Proc. Natl. Acad. Sci. USA.* **104**: 14658–14663.
27. Wang, M. C., W. Min, C. W. Freudiger, G. Ruvkun, and X. S. Xie. 2011. RNAi screening for fat regulatory genes with SRS microscopy. *Nat. Methods.* **8**: 135–138.
28. Cox, G., E. Kable, A. Jones, I. Fraser, F. Manconi, and M. D. Gorrell. 2003. 3-Dimensional imaging of collagen using second harmonic generation. *J. Struct. Biol.* **141**: 53–62.
29. Dombeck, D. A., K. A. Kasischke, H. D. Vishwasrao, M. Ingelsson, B. T. Hyman, and W. W. Webb. 2003. Uniform polarity microtubule assemblies imaged in native brain tissue by second-harmonic generation microscopy. *Proc. Natl. Acad. Sci. USA.* **100**: 7081–7086.
30. Rehberg, M., F. Krombach, U. Pohl, and S. Dietzel. 2011. Label-free 3D visualization of cellular and tissue structures in intact muscle with second and third harmonic generation microscopy. *PLoS One.* **6**: e28237.
31. Zhuo, S., J. Yan, G. Chen, H. Shi, X. Zhu, J. Lu, J. Chen, and S. Xie. 2012. Label-free imaging of basement membranes differentiates normal, precancerous, and cancerous colonic tissues by second-harmonic generation microscopy. *PLoS One.* **7**: e38655.
32. Débarre, D., W. Supatto, and E. Beaurepaire. 2005. Structure sensitivity in third-harmonic generation microscopy. *Opt. Lett.* **30**: 2134–2136.
33. Campagnola, P. J., and L. M. Loew. 2003. Second-harmonic imaging microscopy for visualizing biomolecular arrays in cells, tissues and organisms. *Nat. Biotechnol.* **21**: 1356–1360.
34. Olivier, N., M. A. Luengo-Oroz, L. Duloquin, E. Faure, T. Savy, I. Veilleux, X. Solinas, D. Debarre, P. Bourguine, A. Santos, et al. 2010. Cell lineage reconstruction of early zebrafish embryos using label-free nonlinear microscopy. *Science.* **329**: 967–971.
35. Witte, S., A. Negrean, J. C. Lodder, C. P. de Kock, G. Testa Silva, H. D. Mansvelter, and M. Louise Groot. 2011. Label-free live brain imaging and targeted patching with third-harmonic generation microscopy. *Proc. Natl. Acad. Sci. USA.* **108**: 5970–5975.
36. Débarre, D., W. Supatto, A. M. Pena, A. Fabre, T. Tordjmann, L. Combettes, M. C. Schanne-Klein, and E. Beaurepaire. 2006. Imaging lipid bodies in cells and tissues using third-harmonic generation microscopy. *Nat. Methods.* **3**: 47–53.
37. Mari, M., G. Filippidis, K. Palikaras, B. Petanidou, C. Fotakis, and N. Tavernarakis. 2015. Imaging ectopic fat deposition in *Caenorhabditis elegans* muscles using nonlinear microscopy. *Microsc. Res. Tech.* **78**: 523–528.
38. Tsevelakis, G. J., E. V. Megalou, G. Filippidis, B. Petanidou, C. Fotakis, and N. Tavernarakis. 2014. Label-free imaging of lipid depositions in *C. elegans* using third-harmonic generation microscopy. *PLoS One.* **9**: e84431.
39. Brenner, S. 1974. The genetics of *Caenorhabditis elegans*. *Genetics.* **77**: 71–94.
40. Samara, C., P. Syntichaki, and N. Tavernarakis. 2008. Autophagy is required for necrotic cell death in *Caenorhabditis elegans*. *Cell Death Differ.* **15**: 105–112.
41. Barros, A. G., J. Liu, G. A. Lemieux, B. C. Mullaney, and K. Ashrafi. 2012. Analyses of *C. elegans* fat metabolic pathways. *Methods Cell Biol.* **107**: 383–407.
42. McKay, R. M., J. P. McKay, L. Avery, and J. M. Graff. 2003. *C. elegans*: a model for exploring the genetics of fat storage. *Dev. Cell.* **4**: 131–142.
43. Herndon, L. A., P. J. Schmeissner, J. M. Dudaronek, P. A. Brown, K. M. Listner, Y. Sakano, M. C. Paupard, D. H. Hall, and M. Driscoll. 2002. Stochastic and genetic factors influence tissue-specific decline in ageing *C. elegans*. *Nature.* **419**: 808–814.
44. Borg, M. L., S. F. Omran, J. Weir, P. J. Meikle, and M. J. Watt. 2012. Consumption of a high-fat diet, but not regular endurance exercise training, regulates hypothalamic lipid accumulation in mice. *J. Physiol.* **590**: 4377–4389.
45. Liu, L., K. Zhang, H. Sandoval, S. Yamamoto, M. Jaiswal, E. Sanz, Z. Li, J. Hui, B. H. Graham, A. Quintana, et al. 2015. Glial lipid droplets and ROS induced by mitochondrial defects promote neurodegeneration. *Cell.* **160**: 177–190.
46. Oikonomou, G., and S. Shaham. 2011. The glia of *Caenorhabditis elegans*. *Glia.* **59**: 1253–1263.
47. Stout, R. F., Jr., A. Verkhatsky, and V. Parpura. 2014. *Caenorhabditis elegans* glia modulate neuronal activity and behavior. *Front. Cell Neurosci.* **8**: 67.
48. Pitt, J. N., and M. Kaerberlein. 2015. Why is aging conserved and what can we do about it? *PLoS Biol.* **13**: e1002131.
49. Huffman, D. M., and N. Barzilai. 2009. Role of visceral adipose tissue in aging. *Biochim. Biophys. Acta.* **1790**: 1117–1123.
50. Muzumdar, R., D. B. Allison, D. M. Huffman, X. Ma, G. Atzmon, F. H. Einstein, S. Fishman, A. D. Poduval, T. McVei, S. W. Keith, et al. 2008. Visceral adipose tissue modulates mammalian longevity. *Ageing Cell.* **7**: 438–440.
51. Barzilai, N., D. M. Huffman, R. H. Muzumdar, and A. Bartke. 2012. The critical role of metabolic pathways in aging. *Diabetes.* **61**: 1315–1322.
52. Colman, R. J., R. M. Anderson, S. C. Johnson, E. K. Kastman, K. J. Kosmatka, T. M. Beasley, D. B. Allison, C. Cruzen, H. A. Simmons, J. W. Kemnitz, et al. 2009. Caloric restriction delays disease onset and mortality in rhesus monkeys. *Science.* **325**: 201–204.
53. Masoro, E. J. 2005. Overview of caloric restriction and ageing. *Mech. Ageing Dev.* **126**: 913–922.
54. Lakowski, B., and S. Hekimi. 1998. The genetics of caloric restriction in *Caenorhabditis elegans*. *Proc. Natl. Acad. Sci. USA.* **95**: 13091–13096.
55. Lapiere, L. R., C. D. De Magalhaes Filho, P. R. McQuary, C. C. Chu, O. Visvikis, J. T. Chang, S. Gelino, B. Ong, A. E. Davis, J. E. Irazoqui,

- et al. 2013. The TFEB orthologue HLH-30 regulates autophagy and modulates longevity in *Caenorhabditis elegans*. *Nat. Commun.* **4**: 2267.
56. Settembre, C., C. Di Malta, V. A. Polito, M. Garcia Arencibia, F. Vetrini, S. Erdin, S. U. Erdin, T. Huynh, D. Medina, P. Colella, et al. 2011. TFEB links autophagy to lysosomal biogenesis. *Science*. **332**: 1429–1433.
57. Cuervo, A. M. 2011. Cell biology. Autophagy's top chef. *Science*. **332**: 1392–1393.
58. Lionaki, E., M. Markaki, K. Palikaras, and N. Tavernarakis. 2015. Mitochondria, autophagy and age-associated neurodegenerative diseases: new insights into a complex interplay. *Biochim. Biophys. Acta*. **1847**: 1412–1423.
59. Lapierre, L. R., M. J. Silvestrini, L. Nunez, K. Ames, S. Wong, T. T. Le, M. Hansen, and A. Melendez. 2013. Autophagy genes are required for normal lipid levels in *C. elegans*. *Autophagy*. **9**: 278–286.
60. Hansen, M., A. Chandra, L. L. Mitic, B. Onken, M. Driscoll, and C. Kenyon. 2008. A role for autophagy in the extension of lifespan by dietary restriction in *C. elegans*. *PLoS Genet.* **4**: e24.
61. Folick, A., H. D. Oakley, Y. Yu, E. H. Armstrong, M. Kumari, L. Sanor, D. D. Moore, E. A. Ortlund, R. Zechner, and M. C. Wang. 2015. Lysosomal signaling molecules regulate longevity in *Caenorhabditis elegans*. *Science*. **347**: 83–86.
62. Lapierre, L. R., S. Gelino, A. Melendez, and M. Hansen. 2011. Autophagy and lipid metabolism coordinately modulate life span in germline-less *C. elegans*. *Curr. Biol.* **21**: 1507–1514.
63. Wang, M. C., E. J. O'Rourke, and G. Ruvkun. 2008. Fat metabolism links germline stem cells and longevity in *C. elegans*. *Science*. **322**: 957–960.
64. Settembre, C., R. De Cegli, G. Mansueto, P. K. Saha, F. Vetrini, O. Visvikis, T. Huynh, A. Carissimo, D. Palmer, T. J. Klisch, et al. 2013. TFEB controls cellular lipid metabolism through a starvation-induced autoregulatory loop. *Nat. Cell Biol.* **15**: 647–658.
65. Seah, N. E., C. D. de Magalhaes Filho, A. P. Petrashen, H. R. Henderson, J. Laguer, J. Gonzalez, A. Dillin, M. Hansen, and L. R. Lapierre. 2016. Autophagy-mediated longevity is modulated by lipoprotein biogenesis. *Autophagy*. **12**: 261–272.
66. Steinbaugh, M. J., S. D. Narasimhan, S. Robida-Stubbs, L. E. Moronetti Mazzeo, J. M. Dreyfuss, J. M. Hourihan, P. Raghavan, T. N. Operana, R. Esmailie, and T. K. Blackwell. 2015. Lipid-mediated regulation of SKN-1/Nrf in response to germ cell absence. *eLife*. **4**: e07836.
67. Houtkooper, R. H., C. Argmann, S. M. Houten, C. Canto, E. H. Jeninga, P. A. Andreux, C. Thomas, R. Doenlen, K. Schoonjans, and J. Auwerx. 2011. The metabolic footprint of aging in mice. *Sci. Rep.* **1**: 134.
68. Kolovou, G., N. Katsiki, A. Pavlidis, H. Bilianou, G. Goumas, and D. P. Mikhailidis. 2014. Ageing mechanisms and associated lipid changes. *Curr. Vasc. Pharmacol.* **12**: 682–689.
69. Furuno, T., T. Kannb, K. Arita, M. Asami, T. Utsumi, Y. Doi, M. Inoue, and K. Utsumi. 2001. Roles of long chain fatty acids and carnitine in mitochondrial membrane permeability transition. *Biochem. Pharmacol.* **62**: 1037–1046.
70. Piro, S., M. Anello, C. Di Pietro, M. N. Lizzio, G. Patane, A. M. Rabuazzo, R. Vigneri, M. Purrello, and F. Purrello. 2002. Chronic exposure to free fatty acids or high glucose induces apoptosis in rat pancreatic islets: possible role of oxidative stress. *Metabolism*. **51**: 1340–1347.
71. Scorrano, L., D. Penzo, V. Petronilli, F. Pagano, and P. Bernardi. 2001. Arachidonic acid causes cell death through the mitochondrial permeability transition. Implications for tumor necrosis factor- α apoptotic signaling. *J. Biol. Chem.* **276**: 12035–12040.
72. Wrede, C. E., L. M. Dickson, M. K. Lingohr, I. Briaud, and C. J. Rhodes. 2002. Protein kinase B/Akt prevents fatty acid-induced apoptosis in pancreatic beta-cells (INS-1). *J. Biol. Chem.* **277**: 49676–49684.
73. Inloes, J. M., K. L. Hsu, M. M. Dix, A. Viader, K. Masuda, T. Takei, M. R. Wood, and B. F. Cravatt. 2014. The hereditary spastic paraplegia-related enzyme DDHD2 is a principal brain triglyceride lipase. *Proc. Natl. Acad. Sci. USA*. **111**: 14924–14929.
74. Rainier, S., M. Bui, E. Mark, D. Thomas, D. Tokarz, L. Ming, C. Delaney, R. J. Richardson, J. W. Albers, N. Matsunami, et al. 2008. Neuropathy target esterase gene mutations cause motor neuron disease. *Am. J. Hum. Genet.* **82**: 780–785.
75. Sanhueza, M., A. Chai, C. Smith, B. A. McCray, T. I. Simpson, J. P. Taylor, and G. Pennetta. 2015. Network analyses reveal novel aspects of ALS pathogenesis. *PLoS Genet.* **11**: e1005107.
76. Tesson, C., M. Nawara, M. A. Salih, R. Rossignol, M. S. Zaki, M. Al Balwi, R. Schule, C. Mignot, E. Obre, A. Bouhouche, et al. 2012. Alteration of fatty-acid-metabolizing enzymes affects mitochondrial form and function in hereditary spastic paraplegia. *Am. J. Hum. Genet.* **91**: 1051–1064.
77. Testa, G., F. Biasi, G. Poli, and E. Chiarotto. 2014. Calorie restriction and dietary restriction mimetics: a strategy for improving healthy aging and longevity. *Curr. Pharm. Des.* **20**: 2950–2977.
78. Morley, J. E. 2004. The metabolic syndrome and aging. *J. Gerontol. A Biol. Sci. Med. Sci.* **59**: 139–142.
79. Koster, A., S. Stenholm, D. E. Alley, L. J. Kim, E. M. Simonsick, A. M. Kanaya, M. Visser, D. K. Houston, B. J. Nicklas, F. A. Tylavsky, et al. 2010. Body fat distribution and inflammation among obese older adults with and without metabolic syndrome. *Obesity (Silver Spring)*. **18**: 2354–2361.
80. Visvikis, O., N. Ihuegbu, S. A. Labeled, L. G. Luhachack, A. M. Alves, A. C. Wollenberg, L. M. Stuart, G. D. Stormo, and J. E. Irazoqui. 2014. Innate host defense requires TFEB-mediated transcription of cytoprotective and antimicrobial genes. *Immunity*. **40**: 896–909.